for a limited set of multipole terms selected on the basis of the symmetry characteristics of the nearest-neighbour geometry alone will not be justified. In the structure described here, for example, the radial dependence in the regions of excess and deficient density near the Cu atom differ markedly. An efficient multipole representation of the density in terms of a limited set of angular and radial functions, based on the usual assumption that the electron density near each nucleus may be described as a separable sum of products of radial and angular functions, would almost certainly not be possible either in this or in other analogous cases. Theoretical studies are needed to complement this work, if only to confirm the magnitude of the effects involved.

Financial support for this project was provided by the Australian Research Grants Scheme and by the Research Committee of the University of Western Australia. One of us (NS) acknowledges receipt of a Commonwealth Postgraduate Award.

References

BECKER, P. J., COPPENS, P. & HIRSHFELD, F. L. (1984). *J. Appl. Cryst.* **17**, 369.
COPPENS, P. (1984). *Acta Cryst.* A**40**, 184-195.
CROMER, D. T. & LIBERMAN, D. (1970). *J. Chem. Phys.* **53**, 1891-1898.
CROMER, D. T. & MANN, J. B. (1968). *Acta Cryst.* A**24**, 321-324.
DAWSON, B. (1967). *Proc. R. Soc. London Ser. A*, **298**, 264-288.
DUNITZ, J. D. & SEILER, P. (1983). *J. Am. Chem. Soc.* **105**, 7056-7058.
FIGGIS, B. N., REYNOLDS, P. A., WHITE, A. H. & WILLIAMS, G. A. (1981). *J. Chem. Soc. Dalton Trans.* pp. 371-376.
FLACK, H. D. (1977). *Acta Cryst.* A**33**, 890-898.
FRENCH, S. & WILSON, K. (1978). *Acta Cryst.* A**34**, 517-525.
HEALY, P. C. & WHITE, A. H. (1972). *J. Chem. Soc. Dalton Trans.* pp. 1913-1917.
HERMANSSON, K. (1985). *Acta Cryst.* B**41**, 161-169.
JAHN, H. A. & TELLER, E. (1937). *Proc. R. Soc. London Ser. A*, **161**, 220-235.
LARSON, A. C. (1970). *Crystallographic Computing*, edited by F. R. AHMED. Copenhagen: Munksgaard.
MARUMO, F., ISOBE, M., SAITO, Y., YAGI, T. & AKIMOTO, S. (1974). *Acta Cryst.* B**30**, 1904-1906.
MASLEN, E. N., SPADACCINI, N. & WATSON, K. J. (1983). *Proc. Indian Acad. Sci.* **92**, 443-448.
MITSCHLER, A., REES, B. & LEHMANN, M. S. (1978). *J. Am. Chem. Soc.* **100**, 3390-3397.
PAULI, W. (1925). *Z. Phys.* **31**, 765.
PRICE, P. F. & MASLEN, E. N. (1978). *Acta Cryst.* A**34**, 173-183.
REES, B. (1976). *Acta Cryst.* A**32**, 483-488.
STEWART, J. M. & HALL, S. R. (1983). *The XTAL System of Crystallographic Programs.* Tech. Rep. TR-1364.1. Computer Science Center, Univ. of Maryland, College Park, Maryland.
TANAKA, K., KONISHI, M. & MARUMO, F. (1979). *Acta Cryst.* B**35**, 1303-1308.
TANAKA, K. & MARUMO, F. (1982). *Acta Cryst.* B**38**, 1422-1427.
VARGHESE, J. N. & MASLEN, E. N. (1985). *Acta Cryst.* B**41**, 184-190.
WANG, Y. & COPPENS, P. (1976). *Inorg. Chem.* **15**, 1122-1127.
WILSON, A. J. C. (1949). *Acta Cryst.* **2**, 318-321.

Acta Cryst. (1986). B**42**, 436-442

X-ray Diffraction Study of Short-Range-Ordered Structure in a Disordered Ag–15·0 at.% Mg Alloy

BY KEN-ICHI OHSHIMA* AND JIMPEI HARADA

Department of Applied Physics, Nagoya University, Nagoya 464, *Japan*

(*Received* 24 *January* 1986; *accepted* 25 *March* 1986)

Abstract

Short-range-order (SRO) parameters of disordered Ag–15·0 at.% Mg alloy were determined at room temperature from an analysis of the X-ray diffuse scattering by applying the Borie & Sparks [*Acta Cryst.* (1971), A**27**, 198-201] separation method. The SRO parameters beyond the 20th-neighbor shell were found to play an important role in characterizing a fourfold splitting of the diffuse scattering. Computer-simulated local Mg-atom arrangement in a f.c.c. lattice showed the existence of Cu_3Au-type ordered regions of one or two unit-cell dimensions connected with antiphase relations. Comparison of the atomic-pair interaction potential obtained from the SRO diffuse scattering and the form of the long-range interaction attributed to conduction-electron screening of the ions led to the deduction that the Fermi surface of this alloy has some resemblance to that of a noble metal.

1. Introduction

Characteristic fourfold splittings of diffuse scattering have been observed at the 100, 110 and equivalent positions on the electron and X-ray diffraction patterns from disordered or quenched states of several binary alloys with a face-centered cubic structure [Cu-Au: Raether (1954); Sato, Watanabe & Ogawa

* Present address: Institute of Applied Physics, University of Tsukuba, Sakura, Ibaraki 305, Japan.

0108-7681/86/050436-07$01.50

(1962); Marcinkowski & Zwell (1963); Watanabe & Fisher (1965); Moss (1969); Hashimoto & Ogawa (1970); Yamagishi, Hashimoto & Iwasaki (1982); Bessière, Lefebvre & Calvayrac (1983); Ohshima, Harada & Moss (1986); Cu–Al: Scattergood, Moss & Bever (1970); Cu–Pd: Watanabe (1959); Ohshima, Watanabe & Harada (1976); Cu–Pd and Cu–Pt: Ohshima & Watanabe (1973); Ag–Mg, Au–Pd and Au–Zn: Ohshima & Watanabe (1977); Au–Pd: Lin, Spruiell & Williams (1970)]. The split diffuse maxima correspond to the intersections of slightly curved diffuse streaks around the 100 and 110 positions and their separation varies monotonically with increasing alloy content. The result has been interpreted as an imaging effect of a flat Fermi surface normal to the ⟨110⟩ directions predicted by Moss (1969) and Krivoglaz (1969).

The X-ray analysis of the diffuse scattering with such a fine structure was performed for a disordered Cu–29·8 at.% Pd alloy (Ohshima, Watanabe & Harada, 1976) and the atomic-pair interaction potential ratios were obtained on the basis of the Clapp & Moss (1966) theory. A comparison was made between the results and the form of long-range oscillatory potential predicted by the conduction-electron screening model.

As for the α-phase Ag–Mg alloy which also forms f.c.c. structure for compositions up to 28 at.% Mg (Hansen & Anderko, 1958), conspicuous diffuse rods are observed on the diffraction pattern parallel to the h and k axes through $h10$, $h30$, ... and $1k0$, $3k0$, ..., besides the split diffuse maxima (Ohshima & Watanabe, 1977). A typical electron diffraction pattern from a disordered Ag–19·0 at.% Mg alloy is shown in Fig. 1. It is of interest to see what sort of short-range ordering is associated with this diffuse scattering.

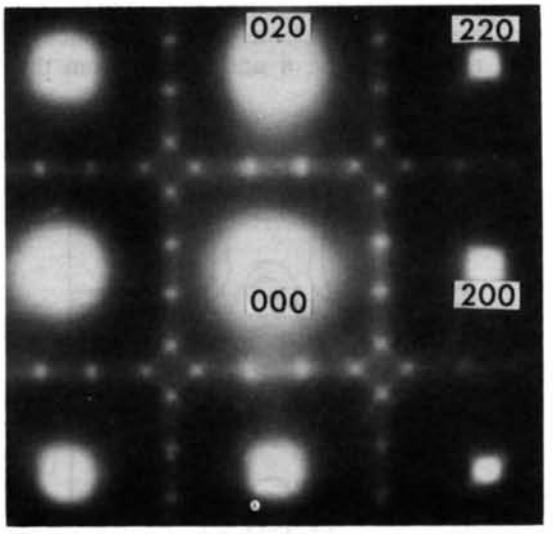

Fig. 1. Electron diffraction pattern from disordered Ag–19·0 at.% Mg alloy quenched from 770 K. The incident beam is parallel to [001] of the fundamental lattice.

In the present study, the X-ray diffuse scattering from an Ag–15·0 at.% Mg alloy sample quenched from 770 K was measured at room temperature and the separation of the short-range-order (SRO) diffuse scattering from the other sources of diffuse scattering was made with the Borie–Sparks method (Borie & Sparks, 1971). Some of the results obtained with this analysis have been reported briefly (Ohshima & Harada, 1979). In this paper we give a full description of the analysis of diffuse scattering and the determination of SRO parameters. A local atomic arrangement simulated by computer and based on these SRO parameters is discussed in connection with the peculiar diffuse scattering. The shape of the Fermi surface is also discussed by comparing the atomic-pair interaction potential ratios, which are obtained from the present analysis, with those attributed to the screening effect of conduction electrons.

2. Experimental procedures and data analysis

2.1. *Sample preparation*

A single crystal was grown by the Bridgeman technique. Purity of the starting materials was 99·99% for Ag and Mg. A plate crystal 7 mm in diameter and 2 mm thick was cut from the ingot parallel to the (210) plane. It was chemically etched in HNO_3 solution to remove the distorted surface layer. The specimen was annealed in a graphite crucible inside a silica tube, filled with argon gas, at 770 K for 11 d. This procedure was found to be effective to prevent the evaporation of Mg. The surface was chemically etched again to remove the oxide layer. The lattice parameter of the specimen quenched from 770 K was measured as 4·101 (1) Å. This value corresponds to a composition of 15·0 (8) at.% Mg according to the lattice parameter *vs* composition relation (Fujiwara, Hirabayashi, Watanabe & Ogawa, 1958).

2.2. *X-ray intensity measurements and data analysis*

The X-ray intensity measurements were made by the same procedure as described in the previous study of a disordered Cu–29·8 at.% Pd alloy (Ohshima, Watanabe & Harada, 1976). It should be mentioned that the horizontal and vertical divergences of the incident beam were 0·7 and 0·8°, respectively, so that the resolution in reciprocal space was much better than that of the previous study (Ohshima, Watanabe & Harada, 1976). The power of the incident beam was $1{\cdot}5\,(1)\times10^8$ photons s^{-1} which was estimated with the intensity scattered from polystyrene (C_8H_8) at $2\theta = 100°$.

The volume in reciprocal space over which the diffuse intensity measurement was made is also the same as the previous study (Ohshima, Watanabe &

Harada, 1976) and corresponds to the regions given by Borie & Sparks (1971). The volume was scanned with an interval of $\Delta h_i = 1/40$ for the region where the diffuse maxima were observed and with an interval of $\Delta h_i = 1/20$ for the other regions, in terms of the distance between the 000 and 200 fundamental spots. Air scattering and Bragg intensity near the fundamental spots were subtracted from the observed intensity data.

The diffuse scattering intensity distribution on the ($hk0$) reciprocal-lattice plane is shown in Fig. 2 where the contribution from Compton scattering was also subtracted. As seen from Fig. 2, asymmetry of the diffuse scattering around 110 is not so pronounced that the effect of different atomic sizes for the two species is not serious in the separation of SRO diffuse scattering from total diffuse scattering.

The SRO diffuse scattering was then obtained by removing other diffuse scattering, *i.e.* size-effect modulation and Huang scattering+TDS, from the total diffuse scattering by the Borie & Sparks (1971) method. The SRO intensity distribution on the ($hk0$) reciprocal-lattice plane obtained by this procedure is shown in Fig. 3. A fourfold splitting of the diffuse scattering at the 110 position and the diffuse streaks parallel to the h and k axes through $h10$ and $1k0$ can be clearly seen. The pattern is qualitatively in good agreement with the electron diffraction pattern (Fig. 1), although the alloy content is slightly different. The separation of split diffuse maxima m, defined by Fig. 3, was 0·15 (1) with respect to the distance between the two fundamental spots 000 and 200, which is also in good agreement with 0·147 (5) given by electron diffraction observation (Ohshima & Watanabe, 1977).

3. SRO parameters

Fourier inversion of the SRO diffuse scattering intensity gives the Warren-Cowley SRO parameters α_{lmn}. We have determined them up to the 47th shell. They are listed in Table 1 and plotted against atomic distance r_{lmn} $[=(l^2+m^2+n^2)^{1/2}]$ in Fig. 4. As expected from the general tendency of SRO diffuse scattering α_{lmn} decreases with increasing r_{lmn}.

In order to assess the reliability of the α_{lmn} parameters obtained in this way the SRO diffuse intensity map was synthesized with the parameters determined. It was found that the first 13 α_{lmn} parameters are not sufficient to reproduce the characteristic fourfold diffuse maxima near the 110 point and at least 22 parameters are needed. This result suggests that signs and magnitudes of α_{lmn} parameters with higher indices play an important role in the appearance of split diffuse maxima, although their absolute values are very small. This characteristic of SRO parameters is exactly the same as that found in the SRO analysis of disordered Cu-29·8 at.% Pd alloy (Ohshima, Watanabe & Harada, 1976).

The fact that the absolute values are about half those for the Cu-Pd alloy indicates that the Mg atom arrangement in the f.c.c. lattice is much closer to the disordered state than the case of the Cu-Pd alloy. It is also noticed that α_{200}, α_{400}, α_{600} and α_{800} are all positive while α_{110} and α_{310} are negative and their absolute values are relatively conspicuous compared with the other parameters. This is the same tendency as that found by Suzuki, Harada, Nakashima & Adachi (1982) in their analysis of disordered Au_4Mn alloy, although it is not so pronounced in the present alloy. This fact corresponds to the existence of the diffuse rods along the h and k axes from the 110

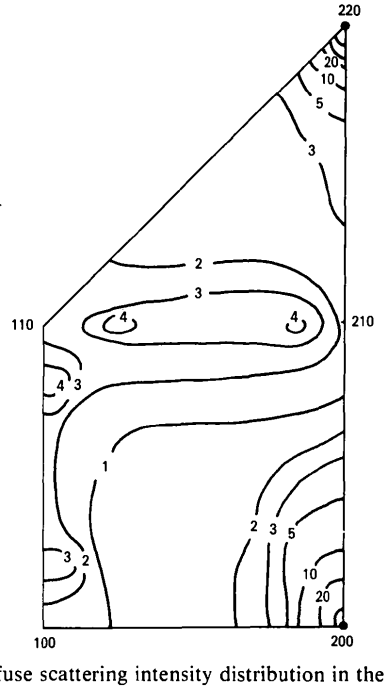

Fig. 2. Diffuse scattering intensity distribution in the ($hk0$) plane of reciprocal space. The quantity plotted is in Laue units.

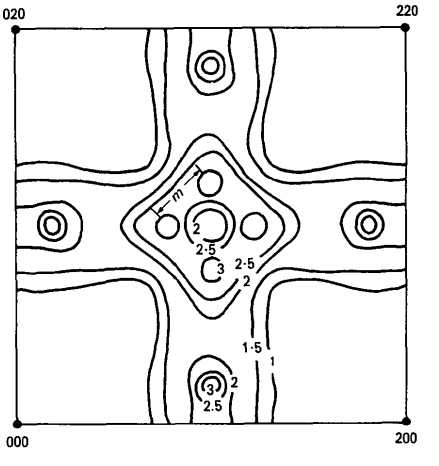

Fig. 3. The short-range-order component of diffuse scattering shown in Fig. 2 in the ($hk0$) plane.

Table 1. *Short-range-order parameters of disordered* Ag–15·0 *at.*% Mg *alloy determined from the Fourier transform of the SRO diffuse scattering intensities and those calculated from the model by computer simulation*

i	*lmn*	Experiment	Simulation	*i*	*lmn*	Experiment
	000	0·958		28	730	−0·001
1	110	−0·069	−0·069	29	732	0·000
2	200	0·113	0·113		651	0·001
3	211	−0·002	−0·002	30	800	0·013
4	220	0·038	0·038	31	811	−0·005
5	310	−0·027	−0·027		741	0·001
6	222	−0·002	−0·002		554	0·001
7	321	0·001	0·001	32	820	0·005
8	400	0·003	0·004		644	−0·003
9	411	0·017	0·017	33	653	0·002
	330	−0·015	−0·015	34	822	0·001
10	420	−0·004	−0·004		660	0·002
11	332	0·000	−0·000	35	831	−0·002
12	422	−0·011	−0·011		750	0·000
13	510	−0·004	−0·004		743	−0·002
	431	0·006	0·006	36	662	0·001
14	521	−0·001	−0·001	37	752	0·000
15	440	0·005	0·004	38	840	−0·002
16	530	−0·002	−0·002	39	910	0·001
	433	0·006	0·006		833	0·002
17	600	0·011	0·010	40	842	−0·001
	442	−0·004	−0·004	41	921	0·000
18	611	−0·001	−0·001		761	−0·001
	532	0·000	0·000		655	0·000
19	620	0·004	0·004	42	664	0·001
20	541	−0·003	−0·003	43	930	0·004
21	622	−0·001			851	−0·001
22	631	0·002			754	0·000
23	444	−0·007		44	932	0·001
24	710	−0·004			763	−0·001
	550	0·000		45	844	−0·002
	543	0·000		46	941	−0·001
25	640	0·001			853	0·002
26	721	−0·001			770	−0·002
	633	0·007		47	860	0·002
	552	0·001			1000	−0·008
27	642	−0·003				

reciprocal-lattice point. It is therefore suggested that the Mg atoms have a tendency to occupy the second-neighbor positions to one another in the f.c.c. lattice.

4. Local atomic arrangement

By using any of the available simulation programs (Gehlen & Cohen, 1965; Bardhan & Cohen, 1976; Williams, 1976; Hirabayashi, Koiwa, Yamaguchi & Kamata, 1978; Suzuki, Harada, Nakashima & Adachi, 1982), a possible local atomic arrangement can be constructed on the basis of observed SRO parameters. Since more than 22 α_{lmn} parameters are needed to reproduce the split diffuse maxima at the 110 point as shown in § 3, a simulation program modified by Suzuki *et al.* (1982) was employed, with which the first 25 SRO parameters can be adjusted to fit the experimentally determined values for the $10\times10\times10$ f.c.c. unit cells. Figs. 5(*a*) and (*b*) show the results of this computer simulation: Fig. 5(*a*) shows the ideally disordered structure in which all the α parameters are zero except $\alpha_{000}=1$; Fig. 5(*b*) shows the observed SRO structure. As in the paper of Suzuki *et al.* (1982), Mg atoms are represented by open circles and are linked together by solid lines in the figures if they are first- or second-nearest neighbors in the f.c.c. lattice. The difference between the SRO state (*b*) and the ideally disordered state (*a*) is not apparent from the figures, although the effect of long-range correlation between any atomic pairs is included in this simulated structure. This is because the α_{lmn} parameters themselves are small, corresponding closely to the disordered state.

The structural difference between the two states, however, can be seen if a careful comparison of the two figures is made. The number of Mg–Mg atom pairs as first neighbors is higher in (*a*) than in (*b*) but the number of Mg–Mg atom pairs as second neighbors in (*b*) is higher than in (*a*). In order to understand this rather intuitive difference between the two figures in a more quantitative way, the numbers of Mg atoms in the first and second shells for each Mg atom were calculated for this simulated structure. The results are summarized in Tables 2(*a*) and (*b*) for ideally disordered and observed SRO structures. In Table 2 the numbers in the third column and the second row are, for example, 39 and 53 for (*a*) and (*b*), respectively. These numbers indicate that 39 and 53 Mg atoms, which have at least one Mg atom in the nearest-neighbor positions and also two Mg atoms in the second-neighbor positions, occur out of 600 atoms in a f.c.c. lattice with $10\times10\times10$ unit cells. The increase from 39 to 53 suggests that such Mg atoms are preferred in the SRO structure. The difference (Table 2*c*) between Tables 2(*b*) and (*a*) shows that the first and second rows are all positive except for the first column, while the third and fourth rows are all negative. This means that Mg atoms have a tendency to occupy the second-neighbor positions rather than the first-neighbor ones so that a Cu_3Au-type ordered structure is likely to be formed. This is related to the fact that the SRO parameters α_{200} and α_{400} are positive while α_{110} and α_{310} are negative. Such a local-order arrangement has been visualized in Fig. 5. Some configurations related to the Cu_3Au-type ordered region are reproduced in Fig. 6, although local compositions are different from the average value, 15 at.% Mg, of the alloy. It should be

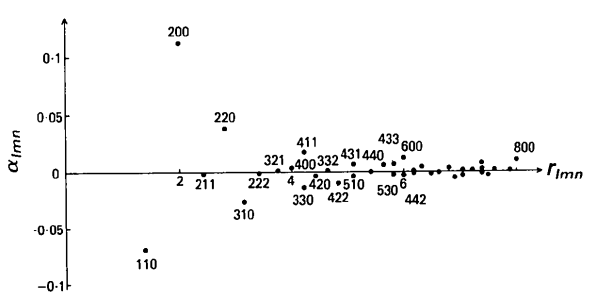

Fig. 4. Short-range-order parameters α_{lmn} *vs* $r_{lmn}=(l^2+m^2+n^2)^{1/2}$.

noticed that antiphase relations exist even in such small ordered regions of two unit cells as indicated by the arrows in Fig. 6. In other words, a local atomic arrangement is characterized by the structure in which a small Cu_3Au-type ordered region of one or two unit-cell dimensions is connected with antiphase relations. However, it is not possible to define the boundary between the local-order region and the disordered matrix in this simulated structure.

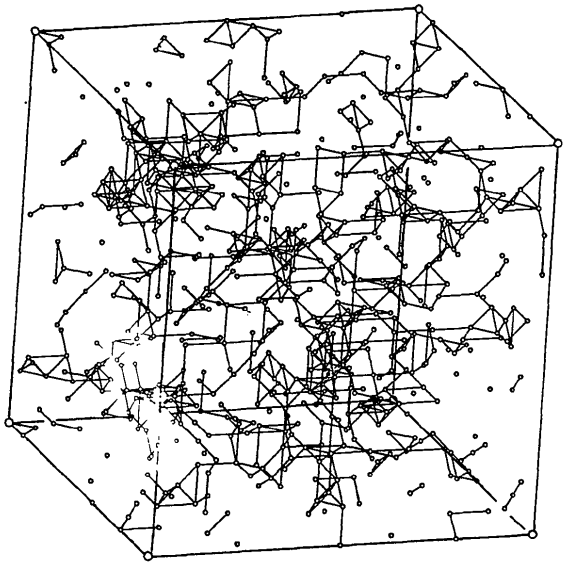

(*a*)

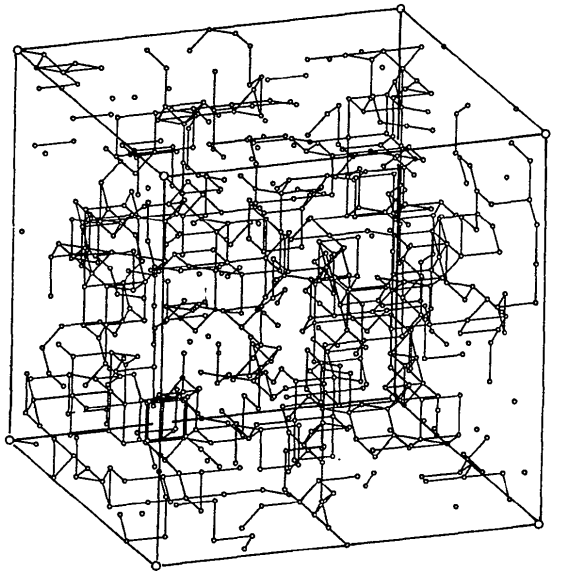

(*b*)

Fig. 5. Three-dimensional distributions of Mg atoms simulated on 10×10×10 f.c.c. unit cells: (*a*) for the ideally disordered state; (*b*) for the observed SRO state of Ag-15·0 at.% Mg alloy. The Mg atoms which are in first- and second-neighbor relations are linked by solid lines.

Table 2. *Joint population of* 110-200 *shells for* Mg *atoms about an* Mg *atom at the origin in the computer-simulated model*

(*a*) Ideally disordered state (RANDOM)

First-nearest neighbor \ Second-nearest neighbor	0	1	2	3	4	5	6	Total
0	28	33	9	2	0	0	0	72
1	57	61	39	7	1	0	0	165
2	95	66	42	10	0	1	0	214
3	33	41	18	8	0	0	0	100
4	14	14	8	2	0	0	0	38
5	4	4	1	0	0	0	0	9
6	1	1	0	0	0	0	0	2
7	0	0	0	0	0	0	0	0
8	0	0	0	0	0	0	0	0
9	0	0	0	0	0	0	0	0
10	0	0	0	0	0	0	0	0
11	0	0	0	0	0	0	0	0
12	0	0	0	0	0	0	0	0
Total	232	220	117	29	1	1	0	600

(*b*) Observed SRO state (SRO25)

First-nearest neighbor \ Second-nearest neighbor	0	1	2	3	4	5	6	Total
0	27	61	57	36	6	3	0	190
1	45	84	53	34	7	2	0	225
2	26	59	36	5	5	0	0	131
3	10	13	19	2	0	0	0	44
4	1	6	2	0	0	0	0	9
5	0	1	0	0	0	0	0	1
6	0	0	0	0	0	0	0	0
7	0	0	0	0	0	0	0	0
8	0	0	0	0	0	0	0	0
9	0	0	0	0	0	0	0	0
10	0	0	0	0	0	0	0	0
11	0	0	0	0	0	0	0	0
12	0	0	0	0	0	0	0	0
Total	109	224	167	77	18	5	0	600

(*c*) SRO25 − RANDOM

First-nearest neighbor \ Second-nearest neighbor	0	1	2	3	4	5	6	Total
0	−1	28	48	34	6	3	0	118
1	−12	23	14	27	6	2	0	60
2	−69	−7	−6	−5	5	−1	0	−83
3	−23	−28	1	−6	0	0	0	−56
4	−13	−8	−6	−2	0	0	0	−29
5	−4	−3	−1	0	0	0	0	−8
6	−1	−1	0	0	0	0	0	−2
7	0	0	0	0	0	0	0	0
8	0	0	0	0	0	0	0	0
9	0	0	0	0	0	0	0	0
10	0	0	0	0	0	0	0	0
11	0	0	0	0	0	0	0	0
12	0	0	0	0	0	0	0	0
Total	−123	4	50	48	17	4	0	0

5. Atomic-pair interaction potential and Fermi surface

The atomic-pair interaction potential $V(\mathbf{r})$ can be obtained with a linearized approximation for the correlation function of a binary alloy (Clapp & Moss, 1966). In this approximation SRO diffuse scattering intensity $I(\mathbf{k})$ is expressed as

$$I(\mathbf{k}) = C/\{1+2x_Ax_B\beta V(\mathbf{k})\}, \qquad (1)$$

where $V(\mathbf{k})$ is a Fourier transform of the atomic-pair interaction potential $V(\mathbf{r})$, defined by $V(\mathbf{r}) = \frac{1}{2}\{V^{AA}(\mathbf{r}) + V^{BB}(\mathbf{r}) - 2V^{AB}(\mathbf{r})\}$, $\mathbf{r}$ being the distance between atom pairs. $\beta = 1/k_BT$ with the Boltzmann

constant k_B and the temperature T. C is a normalization constant. With the same calculation as used by Ohshima, Watanabe & Harada (1976), the atomic-pair interaction potential ratios $V(r_{lmn})/V(r_{110})$ obtained in this way are listed in Table 3 and plotted against r_{lmn} in Fig. 7, where $V(r_{110})$ is the pair-interaction potential between the first-nearest-neighbor atoms and its sign is positive.

It is evident from Fig. 7 that the pair-interaction potential is of long range and oscillates with distance. A comparison was made between the pair potentials obtained and those due to the free-electron screening model (Roth, Zeiger & Kaplan, 1966; Krivoglaz, 1969). The equation used is

$$V(r_{lmn})/V(r_{110}) = A\cos(2k_F a_0 r_{lmn} + \varphi)/(r_{lmn})^3 \quad (2)$$

where k_F is the Fermi-wave vector, φ the phase factor, a_0 the lattice parameter and A a constant. The quantity $2k_F a_0$ is related to the electron/atom ratio as $4{\cdot}911(e/a)^{1/3}$. In the present case e/a is evaluated as 1·15 from the composition, where the number of conduction electrons is assumed to be one for Ag and two for Mg. Flat sections of the Fermi surface are expected to exist normal to the ⟨110⟩ directions according to an electron diffraction study (Ohshima & Watanabe, 1977) as well as the ⟨111⟩ necks which also exist in this alloy, so that the potentials along and close to the ⟨110⟩ and ⟨111⟩ directions are

Table 3. *Values of atomic-pair interaction potential ratios* $V(r_{lmn})/V(r_{110})$

$V(r_{110})$ is the pair-interaction potential between the first-nearest neighbor atoms; its sign is positive.

i	lmn	$V(r_{lmn})/V(r_{110})$	i	lmn	$V(r_{lmn})/V(r_{110})$
1	110	1·000	28	730	0·008
2	200	−1·469	29	732	−0·011
3	211	−0·019		651	−0·034
4	220	−0·336	30	800	−0·143
5	310	0·238	31	811	0·030
6	222	0·167		741	−0·033
7	321	−0·068		554	−0·009
8	400	0·173	32	820	−0·035
9	411	−0·120		644	−0·043
	330	0·134	33	653	−0·017
10	420	0·113	34	822	0·009
11	332	−0·002		660	−0·015
12	422	0·112	35	831	0·023
13	510	−0·066		750	−0·012
	431	−0·003		743	0·033
14	521	0·001	36	662	−0·036
15	440	−0·151	37	752	0·005
16	530	−0·035	38	840	0·069
	433	−0·054	39	910	−0·041
17	600	−0·096		833	−0·013
	442	−0·046	40	842	0·010
18	611	0·050	41	921	−0·004
	532	0·003		761	0·018
19	620	−0·037		655	0·016
20	541	0·078	42	664	−0·043
21	622	−0·016	43	930	−0·080
22	631	−0·013		851	0·029
23	444	0·056		754	0·001
24	710	0·053	44	932	−0·013
	550	−0·008		763	0·009
	543	0·013	45	844	0·044
25	640	0·003	46	941	0·031
26	721	0·018		853	−0·025
	633	−0·088		770	0·044
	552	0·009	47	860	−0·031
27	642	0·034		1000	0·032

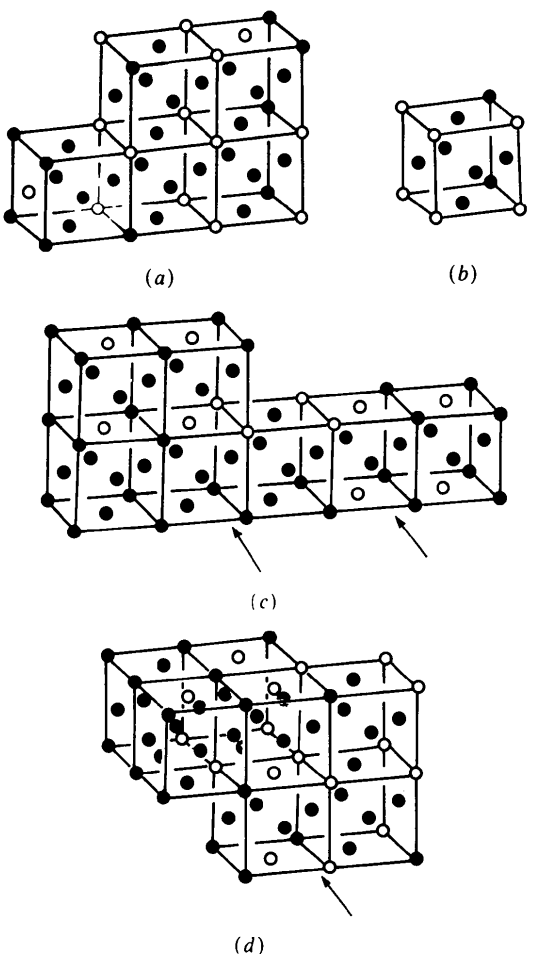

Fig. 6. Several local atom configurations from Fig. 5(*b*). ● and ○ represent Ag and Mg atoms, respectively. The arrows indicate the positions where antiphase relations exist in small ordered regions.

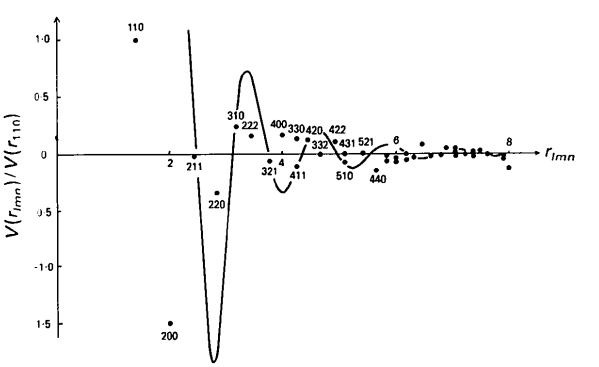

Fig. 7. Atomic-pair interaction potential ratio $V(r_{lmn})/V(r_{110})$ *vs* r_{lmn}. The free-electron screening curve, equation (2), is drawn for comparison.

considered to deviate from the sphere. The pair-interaction potentials along these directions should therefore be excluded from the comparison. Furthermore, the interaction potential between the short-range pair, $V(r_{200})$, should also be excluded because (2) is not valid for such short-range pairs. In Fig. 7, the solid curve is obtained from (2) with $A = 5{\cdot}0$ and $\varphi = 4{\cdot}8$. Agreement between the calculation and the potential ratios observed is satisfactory for medium-range pairs if $V(r_{400})$ is ignored.

The pair interactions along the normal to the flat portions of the Fermi surface should fall off as $(r_{lmn})^{-1}$ (Roth, Zeiger & Kaplan, 1966). The potentials along the ⟨110⟩ directions were then compared with this formula. Since the Fermi sphere is truncated along this direction, the Fermi wave number k'_F along the ⟨110⟩ directions was taken to be $k'_F = tk_F$ where t is the truncation factor representing the flatness of the Fermi surface. For the present alloy composition (Ohshima & Watanabe, 1977) it is estimated to be 0·955. However, the interaction potential along the [110] direction falls off much faster than $(r_{lmn})^{-1}$. This fact may suggest that the Fermi surface normal to the ⟨110⟩ directions is not an ideal plane but truncated.

Grorffy & Stocks (1983) have recently calculated the Fermi surfaces in random metallic alloys on the basis of an energy-band calculation and confirmed the observed concentration dependence of the diffuse scattering maxima in X-ray and electron diffraction patterns for disordered Cu-Pd alloys (Ohshima & Watanabe, 1973; Ohshima, Watanabe & Harada, 1976). They have pointed out that an alloying effect by adding an element with different valence electrons appears in the flatness of the ⟨110⟩ directions in the disordered alloy.

6. Concluding remarks

Recently, Krivoglaz (1983) has discussed the local structure of metallic solid solutions on the basis of the thermodynamical theory. He has shown that a heterogeneous state is stabilized by the large energy gain of the conduction electrons at $2k_F$ even for small ordered regions in the disordered matrix within a certain temperature range. A correlative microdomain model (CMDM), which has been proposed by Hashimoto (1974), is also related to this idea. As far as the atomic arrangement in Fig. 5 is concerned, it is hard to say at this stage that there exists such a heterogeneity in the short-range-ordered structure of this alloy because it is difficult to define the boundaries between the ordered region and disordered matrix, as mentioned above. It is, however, possible to analyze SRO parameters on the basis of a CMDM model if a few assumptions are made, as previously shown by the present authors (Ohshima & Harada, 1981).

References

BARDHAN, P. & COHEN, J. B. (1976). *Acta Cryst.* A**32**, 597-614.

BESSIÈRE, M., LEFEBVRE, S. & CALVAYRAC, Y. (1983). *Acta Cryst.* B**39**, 145-153.

BORIE, B. & SPARKS, C. J. (1971). *Acta Cryst.* A**27**, 198-201.

CLAPP, P. C. & MOSS, S. C. (1966). *Phys. Rev.* **142**, 418-427.

FUJIWARA, K., HIRABAYASHI, M., WATANABE, D. & OGAWA, S. (1958). *J. Phys. Soc. Jpn*, **13**, 167-174.

GEHLEN, P. C. & COHEN, J. B. (1965). *Phys. Rev. A*, **139**, 844-855.

GRORFFY, B. L. & STOCKS, G. M. (1983). *Phys. Rev. Lett.* **50**, 374-377.

HANSEN, M. & ANDERKO, K. (1958). *Constitution of Binary Alloys*, 2nd ed. New York: McGraw-Hill.

HASHIMOTO, S. (1974). *Acta Cryst.* A**30**, 792-798.

HASHIMOTO, S. & OGAWA, S. (1970). *J. Phys. Soc. Jpn*, **29**, 710-721.

HIRABAYASHI, M., KOIWA, M., YAMAGUCHI, S. & KAMATA, K. (1978). *J. Phys. Soc. Jpn*, **45**, 1591-1598.

KRIVOGLAZ, M. A. (1969). *Theory of X-ray and Thermal Neutron Scattering by Real Crystals.* New York: Plenum.

KRIVOGLAZ, M. A. (1983). *Sov. Phys. JETP*, **57**(1), 205-213.

LIN, W., SPRUIELL, J. E. & WILLIAMS, R. O. (1970). *J. Appl. Cryst.* **3**, 297-305.

MARCINKOWSKI, M. J. & ZWELL, L. (1963). *Acta Metall.* **11**, 373-390.

MOSS, S. C. (1969). *Phys. Rev. Lett.* **22**, 1108-1111.

OHSHIMA, K. & HARADA, J. (1979). *AIP Conf. Proc.* **53**, 289-291.

OHSHIMA, K. & HARADA, J. (1981). *Sci. Rep. Res. Inst. Tohoku Univ. Ser. A*, **29**, Suppl. 1, 123-128.

OHSHIMA, K., HARADA, J. & MOSS, S. C. (1986). *J. Appl. Cryst.* **19**, 276-278.

OHSHIMA, K. & WATANABE, D. (1973). *Acta Cryst.* A**29**, 520-526.

OHSHIMA, K. & WATANABE, D. (1977). *Acta Cryst.* A**33**, 784-788.

OHSHIMA, K., WATANABE, D. & HARADA, J. (1976). *Acta Cryst.* A**32**, 883-892.

RAETHER, H. (1954). *Angew. Phys.* **4**, 53-59.

ROTH, L. M., ZEIGER, H. J. & KAPLAN, T. A. (1966). *Phys. Rev.* **149**, 519-525.

SATO, K., WATANABE, D. & OGAWA, S. (1962). *J. Phys. Soc. Jpn*, **17**, 1647-1651.

SCATTERGOOD, R. O., MOSS, S. C. & BEVER, M. B. (1970). *Acta Metall.* **18**, 1087-1098.

SUZUKI, H., HARADA, J., NAKASHIMA, T. & ADACHI, K. (1982). *Acta Cryst.* A**38**, 522-529.

WATANABE, D. (1959). *J. Phys. Soc. Jpn*, **14**, 436-443.

WATANABE, D. & FISHER, P. M. J. (1965). *J. Phys. Soc. Jpn*, **20**, 2170-2179.

WILLIAMS, R. O. (1976). Report ORNL-5140. Oak Ridge National Laboratory, Tennessee.

YAMAGISHI, K., HASHIMOTO, S. & IWASAKI, H. (1982). *J. Phys. Soc. Jpn*, **51**, 605-611.